Exciton dissociation mechanisms in the polymeric semiconductors poly(9,9-dioctylfluorene) and poly(9,9-dioctylfluorene-co-benzothiadiazole)

Mark A. Stevens, Carlos Silva, David M. Russell, and Richard H. Friend
Cavendish Laboratory, University of Cambridge, Madingley Road, Cambridge CB3 0HE, United Kingdom
(Received 19 September 2000; revised manuscript received 10 January 2001; published 6 April 2001)

We present femtosecond transient absorption measurements on the semiconductor conjugated polymers poly(9,9-dioctylfluorene) (F8) and poly(9,9-dioctylfluorene-co-benzothiadiazole) (F8BT). Detailed photophysical modeling reveals that, in F8, sequential excitation, first to the lowest singlet excited state, and then to a higher-energy state resonant with the pump photon energy, is predominantly responsible for the rapid (<150 fs) dissociation of photoinduced excitons. Resonant sequential excitation accesses high-energy states that can promptly evolve to charged or triplet states. In F8BT, however, we find that sequential excitation plays a lesser role in fast polaron-pair generation, and that exciton bimolecular annihilation can explain the charge population. We suggest that the electrophilic benzothiadiazole groups in F8BT facilitate charge formation by dissociation of the excited state formed by exciton-exciton annihilation. Modeling also reveals that exciton bimolecular annihilation can occur via two separate and competing processes. We find that in F8, the dominant mechanism involves exciton diffusion and collision. In F8BT, however, additional annihilation of spatially separated excitons occurs when they interact through the Förster transfer mechanism, where the critical distance for annihilation in F8BT is 4 nm.

DOI: 10.1103/PhysRevB.63.165213 PACS number(s): 78.47.+p, 78.66.Qn, 78.20.Bh

I. INTRODUCTION

Polyfluorenes have emerged recently as a class of conjugated polymer which show promise for applications in optoelectronics. The prospects of high luminescent efficiency, good charge-transport characteristics,[1] thermal stability, and tunability of physical parameters through chemical modification and copolymerization[2] have made these polymers interesting from a commercial aspect. Many members of the polyfluorene family are high-efficiency blue-emitting materials, which are desirable both because they are required for full-color displays, and because they can act as energy donors in blends with other conjugated polymers. Efficient light-emitting diodes,[3] and photovoltaic diodes[4] based on polyfluorene, have been demonstrated.

The simplest materials in this large class of polymers are those based on a fluorene monomer unit with alkyl side chains to confer solubility. One of the most interesting properties of these materials is their ability to form a liquid crystalline phase.[5–7] This has allowed for the preparation of aligned films, which in turn have been used to produce polarized photoluminescence[5,7] and electroluminescence,[8] and to greatly increase the carrier mobility in the alignment direction.[9] The morphology of the polymers can be modified drastically when they are cooled from the liquid crystalline phase. It was reported[5] that slow cooling allows crystallization to occur, while rapid cooling, or ''quenching,'' results in the morphology of the solid film retaining that of the liquid crystal phase.

In addition to their excellent properties for device applications, polyfluorenes and related materials also provide a convenient system in which to study the effects of film morphology.[10] Modifications to the side chains can have strong effects on the packing structure at the molecular level, without significantly altering the electronic structure of the polymer.

A recent comprehensive study by Kraabel *et al.* showed that in phenylene-based conjugated polymers, two types of photoexcitations are produced; an intrachain exciton, and weakly coupled, interchain polaron pairs, created at the expense of the singlet exciton.[11] Numerous additional ultrafast studies have unambiguously identified singlet excitons as being responsible for the stimulated emission observed from solutions[12,13] and solid films of conjugated polymers.[14–16] More recently, singlet excitons have also been associated with the transient photoinduced absorption band which usually appears around 1.5 eV.[16,17] However, the dynamics of the photoinduced absorption over a large range of wavelengths and at various pumping intensities indicate that other species are also present. These other absorbing species have been variously attributed to triplet excitons,[18] interchain (spatially indirect) excitons,[13,17,19] and excimers.[20]

It has been well documented that at a sufficiently high initial excitation density, the decay rate of singlet excitons is enhanced due to bimolecular annihilation dynamics.[17,21–25] A previous report from our research group showed that exciton bimolecular annihilation is an important source of photoinduced charges in poly-*p*-phenylenevinylene (PPV),[24] as probed by steady-state photocurrent. Exciton-exciton annihilation was modeled extensively,[22–25] but there is still disagreement on the mechanism responsible for such processes. The mechanism for exciton bimolecular annihilation was variably reported in two regimes. The first is diffusion limited,[21,24] where exciton encounter and collision is the rate-limiting process and the bimolecular rate constant is time independent. The second is characterized by a bimolecular rate ''constant'' that contains an explicit time dependence,[17,22,23,25] where dipole-dipole interactions between pairs of excitons lead to a long-range resonance (Förster) energy transfer. The basis for the two mechanisms includes kinetic modeling of femtosecond transient absorption

and photoluminescence data,[17,21–23,25] modeling of intensity-dependent time-integrated photoluminescence data,[21,31] and modeling of intensity-dependent, time-integrated photocurrent in a photovoltaic diode.[24]

A fundamentally important observation has been the high yield of photoinduced charge generation when thin-film conjugated polymers are subjected to femtosecond optical excitation. Using cw excitation, Köhler *et al.* demonstrated that low-lying excited states ($1B_u$ in particular) do not lead to free charges, but that higher B_u states can do so.[26] Moses *et al.* attributed the high polaron yield when exciting the $\pi \rightarrow \pi^*$ transition with femtosecond pulses to a weak Coulombic binding energy of the lowest excited state.[27] In a separate report, we concluded that such a high exciton dissociation yield is the result of sequential excitation during the pumping process, first to the lowest ($1B_u$) exciton, and then to a higher-lying state that is resonant with the pump photon energy.[28] This is consistent with the report by Kraabel *et al.* of intensity-dependent polaron-pair formation.[11] A recent study by Frolov *et al.* showed that sequential excitation steps can be separated in time and photon energy, and that even-parity states can be classified as those that mediate charge transfer (those 1.1 eV above the $1B_u$ state), and those that promptly convert internally to $1B_u$.[29] Finally, recent photocurrent cross-correlation measurements by Müller *et al.* demonstrated that high-lying electronic states generate free photocarriers.[30] In the latter experiment, the increase in photocurrent produced by a pump pulse resonant with the $\pi \rightarrow \pi^*$ transition, when photoexcited with a second variably delayed femtosecond pulse in the near infrared, is measured as a function of delay between the two pulses.

In this paper we present results of a study on the wavelength and pump-intensity dependence of the transient absorption of two polyfluorene derivatives: poly(9,9-dioctylfluorene) (F8) and poly(9,9-dioctylfluorene-co-benzothiadiazole) (F8BT). We identify photogenerated species that are consistent with the unified picture that has been built up for phenylene-based conjugated polymers.[11] Using a detailed photophysical model, we explore the mechanisms of exciton dissociation over a large pump fluence range. In accord with our earlier work on related step-ladder polymers,[28] we find that sequential excitation during the pump pulse can explain the very fast exciton dissociation, which is found to occur in F8. In contrast, exciton-exciton annihilation dominates charge generation in F8BT. Furthermore, we show that exciton-exciton annihilation is an important relaxation pathway in both F8 and F8BT, and that it can occur by the different mechanisms outlined above. In F8, annihilation occurs by exciton collisions where exciton diffusion is the rate-limiting factor. In F8BT, the overlap of photoluminescence (PL) and exciton absorption leads to a Förster interaction, which is the dominant annihilation mechanism. The usual approach to modeling annihilation which occurs via the Förster transfer process relies on the assumption that the annihilation rate is proportional to $t^{-1/2}$. However, as described in the Appendix, this approach masks the underlying physical process involved in Förster energy transfer. One of the aims of the present paper is to describe the Förster annihilation process in a more physically realistic way.

II. EXPERIMENT

Polymers were dissolved in anhydrous *p*-xylene in a nitrogen environment with standard syringe techniques, to avoid contact of either polymer or solvent with air. Films were prepared in a dry nitrogen-filled glove box by spin coating the polymer solution (concentration 1.6 g/ml) onto Spectrosil substrates. For transient absorption spectra, $\sim$100-nm-thick films of F8 were used. For most measurements of dynamics in F8 at specific probe photon energies, $\sim$30-nm-thick films were used in order to prevent waveguiding and amplified spontaneous emission (ASE).[31–33] F8BT films of $\sim$100-nm-thickness were used for all measurements, because no ASE occurs in the samples investigated herein. Samples were stored in the glove box prior to use. During measurements, samples were kept under dynamic vacuum ($<10^{-5}$ mbar) to prevent photo-oxidation. Absorption spectra were measured with a Hewlett-Packard 8453 diode-array spectrophotometer.

Femtosecond pump-probe experiments were performed using a home-built Ti:sapphire laser, based on the design of Kapteyn and Murnane,[34] to produce 20-fs pulses with a central wavelength of 780 nm (1.59 eV) and at a repetition rate of 76 MHz. The pulse train of this laser was synchronized to that of a Coherent Antares 76-s Nd:YAG (yttrium aluminum garnet) laser, which was actively mode locked and also running at 76 MHz. Synchronization was achieved using commercially available fast photodiodes and phase-lock-loop electronics (Time-Bandwidth Products, model CLX-1000) to continuously detect the phase difference between the two pulse trains and adjust the cavity length of the Ti:sapphire laser. This resulted in the phases of the two pulse-trains being locked. Dynamic control of the Ti:sapphire back mirror (high-reflector) allowed the timing of the pulse trains to be matched to within $\sim$3 ps.

Primary amplification of the output from the Ti:sapphire laser took place in a longitudinally pumped three-stage dye amplifier. A recirculating solution of LDS 751 dissolved in propylene carbonate at a concentration of $\sim 5\times10^{-4}$ M was used as the gain medium. The amplifier was pumped using the output of a Nd:YAG regenerative amplifier (Spectron Lasers) (220 μJ, 532 nm, 300-ps pulse duration, 1-kHz repetition rate). The regenerative amplifier was seeded by the output of the Antares laser, and was therefore phase locked to the Ti:sapphire laser. The dye amplifier was run slightly into the saturation regime in order to reduce pulse-to-pulse fluctuations. The pulse energy output from the amplifier was $\sim$5 μJ. Group-velocity dispersion occurring in the amplifier was corrected using a pair of fused silica prisms in a double-pass configuration,[35] thereby compressing the amplified pulses to $\sim$100 fs.

Around 90% of the amplifier output was focused onto a 2-mm-thick sapphire plate to produce a single-filament white-light continuum. The other 10% was amplified in a fourth dye cell (pumped by 70-mW output of the regenerative amplifier). This beam was mechanically chopped at 500

Hz, and frequency doubled in a 0.5-mm β-barium borate (BBO) crystal to give pump pulses at 3.18 eV.

The white-light continuum was spectrally filtered according to how it was to be used. For single-wavelength measurements in the visible, a ''hot mirror'' was used to block the fundamental. For single-wavelength measurements above the fundamental, an RG850 long-pass filter was used. When collecting spectra, a BG7 filter was used to reduced the intensity of the remaining fundamental while still passing the majority of the continuum.

After filtering, the continuum was split, with one beam acting as a reference while the other beam passed through the sample and acted as a probe. The probe was delayed with respect to the pump by means of a computer-controlled delay stage. Pump and probe beams were focused coincidentally onto the polymer sample, with the pump spot typically 125 μm in diameter and the probe 30–50 μm in diameter. The probe and reference beams were dispersed in a 0.25-m spectrometer (Spex). Changes in probe transmission ($\Delta T/T$) at a single wavelength were monitored with a pair of silicon *p-i-n* diodes, and lock-in amplification techniques. Alternatively, $\Delta T/T$ spectra at fixed delays were measured with a peltier-cooled charge-coupled device (CCD) camera (Wright Instruments).

The chirp on the continuum was characterized in two ways. Nonresonant two-photon absorption in a CdS crystal was used to measure the relative temporal position of each of the spectral components of the probe with energies below 1.5 eV. To characterize the chirp at energies greater than 1.5 eV, we measured the spectral position of the onset of photoinduced transmission change in a thin film of F8 for a range of delays between the pump and probe. Any nonuniformity of the rise time with photon energy (<100 fs) is small compared to the time scale of the chirp across the white-light spectrum (several picoseconds). Using the polymer as well as the CdS allowed for a characterization of the chirp over the photon energy range 1.13–3.10 eV. The chirp on the transient absorption spectra was then corrected by applying a numerical deconvolution.

Photoluminescence spectra were measured by pumping the polymer at 3.18 eV, and dispersing the luminescence in the spectrograph and onto the CCD camera. Only time-integrated spectra were measured and no correction for the CCD response was made.

We performed experiments in order to determine whether the pump pulses were of sufficient intensity to depopulate the ground state of the polymers significantly. These experiments involved comparing the intensity of the pump light, which was transmitted through the sample, to the intensity of a reference beam which did not pass through the sample. The reference beam was formed by splitting off a fraction of the main pump beam before it reached the sample. A pair of identical photodiodes was used to measure the intensities of the transmitted and reference beams as a function of pump fluence. Depletion of the ground-state population was then revealed by a nonlinear fluence dependence of the fraction of transmitted pump.

We also explored the possibility of sample photodegradation, which is known to be a severe problem in alkoxy-substituted PPV derivatives, even at moderately low pump intensity.[25] One of the signatures of this irreversible damage is the emergence of transient absorption features and an enhanced exciton density decay rate. We have compared the absorption transients collected with low pump fluence, before and after exposing the film to pump radiation at the highest fluence (350 μJ/cm^2) for a period of 20 min, which is a typical integration time for transients collected at high fluence. The dynamics monitored at several probe photon energies are unaffected by such exposure. Furthermore, the sample was periodically translated to prevent photodegradation effects during long-term exposure ($\gg$20 min at low fluence). Throughout data collection, it was ensured that both the magnitude of the transient absorption signal, and its temporal evolution, did not change with exposure time. All experiments described in this paper were carried out at room temperature.

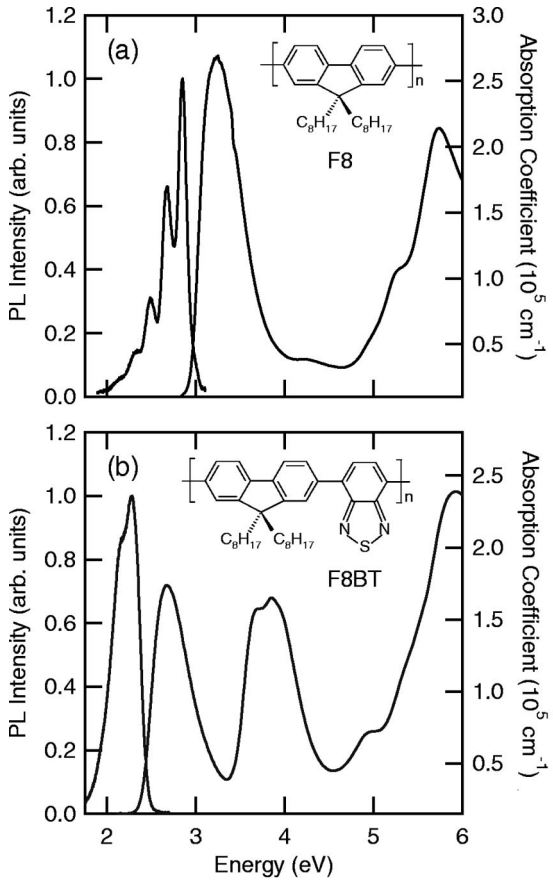

FIG. 1. Absorption and photoluminescence spectra (excitation at 3.18 eV) for thin films of F8 (a), and F8BT (b). The structures of the polymers are shown as insets.

III. RESULTS

A. Absorption and emission spectra

The absorption and PL spectra of F8 and F8BT are shown in Fig. 1. The chemical structures of the two materials are also shown as insets. The PL spectrum of the blue-emitting F8 shows well-defined vibronic structure, with an energy

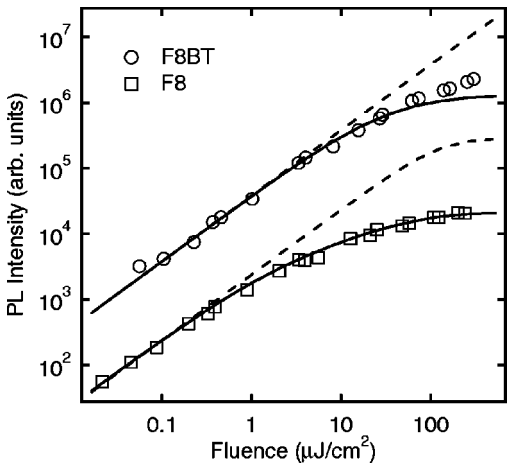

FIG. 2. Intensity of the time-integrated PL as a function of pump pulse energy for F8 (squares) and F8BT (circles). The solid lines show the simulated dependence of the PL intensity on pump energy when exciton-exciton annihilation operates; the dashed lines show the simulated dependence when no annihilation operates. The data have been vertically displaced for clarity.

separation of 0.18 eV between peaks. The largest peak in the PL spectrum of F8 corresponds to the 0-1 transition and is located at 2.85 eV. The 0-0 transition was not visible in any of the F8 films studied here, but has been observed to occur at 2.97 eV in toluene solutions.[36] The PL emission from F8BT, which is centered in the green, is relatively structureless, with two poorly resolved peaks located at 2.28 and 2.15 eV.

The absorption spectrum of F8 is typical of most conjugated polymers. The strong absorption band peaked at 3.24 eV arises from the absorption of light by the delocalized π-electron system of the polymer backbone. This is also the cause of the strong absorption band which peaks at 2.66 eV in the absorption spectrum of F8BT. The higher-energy feature is resolved into a pair of peaks centered at 3.63 and 3.89 eV. Within the measurement limits of our spectrophotometer, none of the F8 films used in the present study showed the small absorption feature which is often seen at around 2.88 eV in this material, and which is assigned to extended chain segments, resulting in higher order.[5,6,36]

Figure 2 shows the frequency- and time-integrated PL intensity from films of F8 (squares) and F8BT (circles) as functions of the pump-pulse fluence. The lines show the results of the photophysical model, details of which are discussed below. The nonlinear intensity dependence at a high pump fluence is attributed to exciton-exciton annihilation becoming a significant pathway for nonradiative decay of the excitons.[14] Saturation of the ground-state absorption occurs only in F8 at fluences greater than 100 μJ/cm^2, and so does not make a significant contribution to the nonlinear behavior shown in Fig. 2.

B. Pump transmission

Figure 3 shows the variation of transmitted pump light as a function of the pump fluence. For both F8 and F8BT the data are shown as markers, while the results of the model are

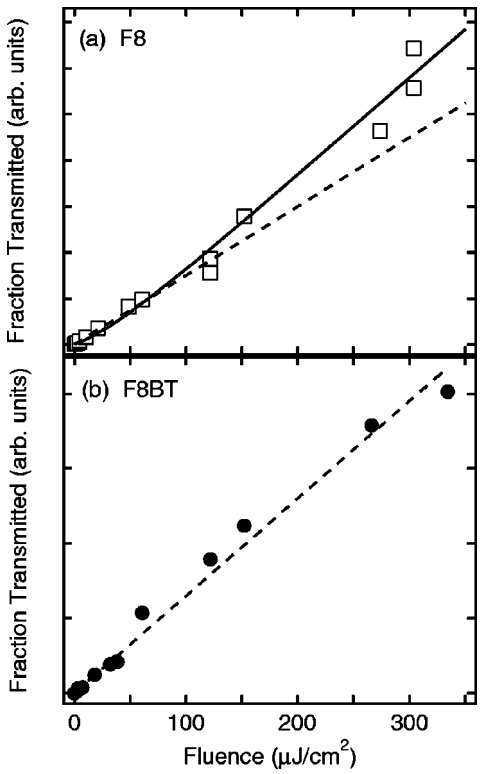

FIG. 3. Fluence dependence of the transmitted pump intensity for F8 (a) and F8BT (b). The data are shown by markers; for F8, the results of the model are shown by the solid line. The dashed lines show the predicted fluence dependence if the ground-state population is very large (i.e., no saturation can occur).

shown as a solid line for F8 only. The dashed lines show the predicted fluence dependence if the ground-state population is sufficiently large that no significant saturation occurs in the experimentally available pump fluence range. For F8, there is a clear nonlinear dependence at high pump fluences, indicating that relatively more pump light is transmitted as the ground state becomes depopulated. As discussed below, using the model to fit these data gives an estimate of the ground-state population density in F8. The linear dependence for F8BT shows that no saturation of the ground state population occurs, even at the highest fluences used here.

C. Transient absorption spectra

Transient absorption spectra at several pump-probe delays for F8, at high and low pump fluences are shown in Fig. 4. These spectra were recorded from 100-nm-thick films which support line-narrowing by ASE.[31–33] Therefore, at a high fluence the exciton signal has already significantly decayed by the earliest delay shown (2 ps).

The early-time spectra are consistent with those reported previously for F8.[11] The positive $\Delta T/T$ signal at high photon energies, which occurs at both high and low pump fluences, appears at the same spectral position as the PL, and so is attributed to probe-induced stimulated emission (SE) of singlet excitons. At low pump fluence (24 μJ/cm^2), we observe stimulated emission with peaks corresponding to the 0-2 and 0-3 vibronic transitions. The SE gives way to a net

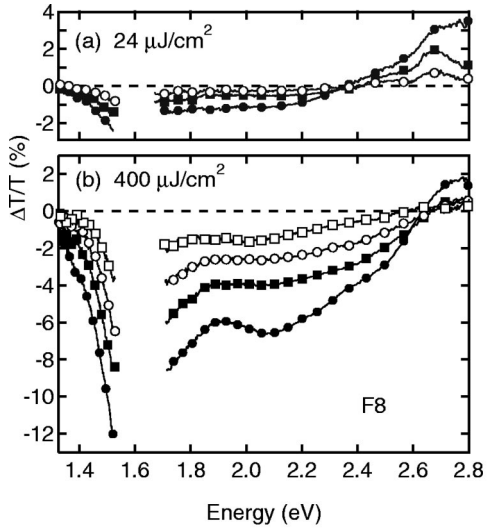

FIG. 4. Transient absorption spectra for F8 at a low pump fluence (a) and a high pump fluence (b) for delays of 2 ps (filled circles), 10 ps (filled squares), 100 ps (open circles), and 600 ps (open squares). Note that the vertical scaling is the same in both panels.

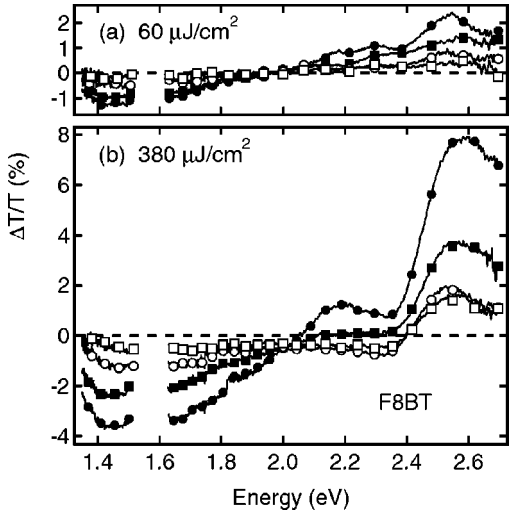

FIG. 5. Transient absorption spectra for F8BT at a low pump fluence (a) and a high pump fluence (b) for delays of 1 ps (filled circles), 10 ps (filled squares), 100 ps (open circles), and 600 ps (open squares). Note that the vertical scaling is the same in both panels.

photoinduced absorption (PA) at energies below 2.35 eV. The relatively weak PA band extends across the rest of the visible spectrum and into the near-IR.

At a high pump fluence, the PA becomes stronger and broader, and overlaps more broadly with the SE. A net positive signal then occurs only at energies greater than 2.65 eV, corresponding to the 0-2 vibronic transition. The shorter-lived SE at high fluence results from efficient exciton depopulation by exciton-exciton annihilation and ASE effects. The dominant feature of the high fluence spectra at all delays is the strong photoinduced absorption. The PA at early times has peaks at approximately 1.5 and 2.1 eV. At long delays, the 2.1-eV PA band is less well resolved, and the spectrum is dominated by a broad PA band which is peaked at around 1.55 eV and extends across most of the visible part of the spectrum. The gap in our spectra from 1.53 to 1.7 eV results from an artifact caused by contamination of the white-light continuum probe by the laser fundamental.

Figure 5 shows the transient absorption spectra for F8BT at high and low pump fluences for a range of delays. The positive signal at energies greater than 2.4 eV in both sets of spectra coincides with the spectral position of the ground-state absorption, and is therefore attributed to a bleaching of the $S_0 \rightarrow S_1$ transition. The smaller positive signal between 2.07 and 2.35 eV, which is present at early times in the high fluence spectra and at all delays in the low fluence spectra, occurs at the same spectral position as the PL, and so is assigned to SE. At a low pump fluence, a net SE signal is observed at all delays in this spectral range, while a weak PA band occurs for photon energies lower than 2.0 eV. In contrast, when a high pump fluence is used, the initial SE is overwhelmed by a very broad PA band after $\sim$10 ps. A rapid reduction of the exciton population by exciton-exciton annihilation and a strong overlapping PA band combine to give a net PA for all long delays. This PA is very long lived, and extends across the visible part of the spectrum and into the near-IR. The crossover point between net gain and loss in the spectrum shifts in time due to the different dynamics of SE and PA. (Note that such a shift is less evident in the high-fluence spectra for F8 shown in Fig. 4.) The ground-state bleach has a very long lifetime, reflecting the slow repopulation of the ground state from the long-lived excited states.

D. Transient absorption dynamics

1. F8

For F8, the time evolution of the transient absorption features have been reported over a short time window (2.5 ps) by Kraabel *et al.*[11] In this paper the transient absorption dynamics of the near-IR PA were monitored at 1.46 eV, the visible PA was monitored at 2.14 eV and the dynamics of the SE were monitored at 2.70 eV. These data are shown for a range of pump fluences in Fig. 6. Markers indicate data, while the solid lines show the results of the model described below. The SE [Fig. 6(a)] and the near-IR PA [Fig. 6(b)] dynamics were measured from films which were below the cutoff thickness for waveguiding,[31] and which therefore did not show spectral line-narrowing by amplification of spontaneous emission. Our absorption transients at all probe photon energy regions are in agreement with those reported by Kraabel *et al.* over short-time windows. The SE and near-IR PA decay dynamics were found to be strongly intensity dependent, but correlated over a large pump fluence range. This PA feature is assigned to absorption of the lowest $(1B_u)$ singlet exciton to a higher-lying state. On the other hand, the evolution of the visible PA signal was found to be intensity independent, and was observed to be slower than the singlet exciton dynamics. However, we note that at the highest pump fluence, the near-IR PA has a very long-lived tail which is absent from the SE dynamics. The visible PA [Fig. 6(c)] was measured from thicker films, which demonstrated

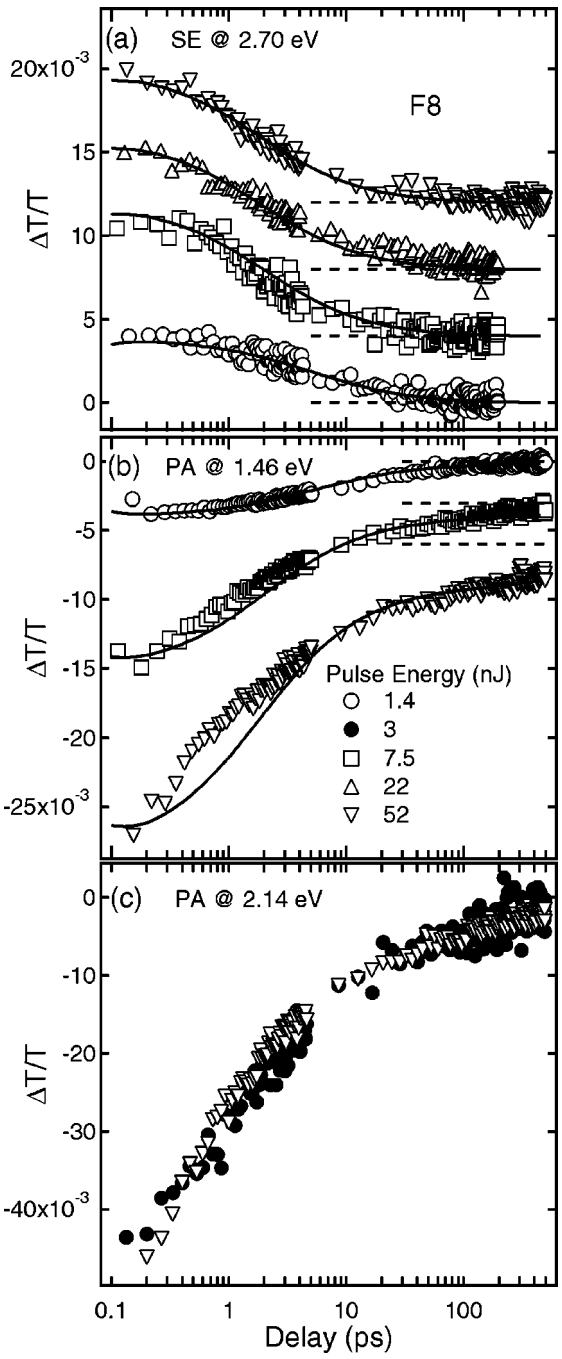

FIG. 6. Transient absorption dynamics of F8 measured from thin (30 nm) films for pump pulse energies shown in the middle panel. (a) shows the SE measured at 2.70 eV, (b) shows the near-IR PA measured at 1.46 eV, and (c) shows the dynamics of the visible PA band measured at 2.14 eV. In (a) and (b) the data have been offset, and the results of the model are shown as solid lines. In (c), the magnitude of the visible PA at low fluence (filled circles) has been scaled by a factor of 10 to match the high-fluence data; this indicates the intensity independence of this band.

line narrowing at a high fluence. Because the dynamics of the PA band that is peaked at 2.1 eV in F8 are independent of the pump intensity over the range used in the present experiments, the dynamics of the visible PA band are unaffected by line narrowing. The visible PA band has an initial

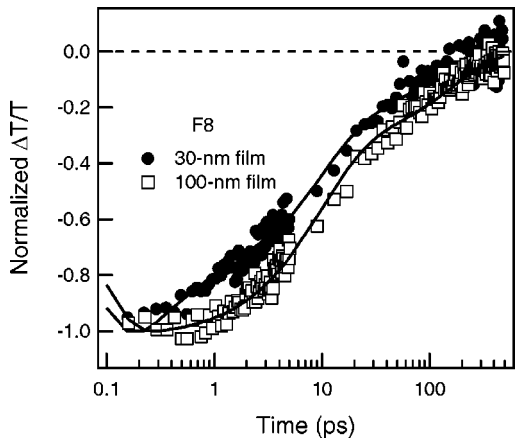

FIG. 7. Comparison of the normalized transient absorption dynamics of a thin film (30 nm, filled circles) and a thicker film (100 nm, open squares) of F8, at a 1.46-eV probe photon energy. The pump fluences were 11.4 and 17 μJ/cm^2, respectively. The solid lines through the data are multiexponential fits convolved with the instrument response function. The amplitude-weighed average time constant from the fits, $\langle\tau\rangle$, is 30 and 62 ps, respectively.

fast decay with a time constant of around 0.9 ps, and a slower decay with a life time of around 80 ps.

Films of varying thickness were necessary in order to both suppress ASE (thin films), and to achieve a sufficient signal-to-noise ratio to map in detail the intensity dependence of the initial $\Delta T/T$ signal (thicker films). It has been shown that the emission spectrum and charge mobility in conjugated polymer thin films is sensitive to the casting spin speed, which determines the solvent evaporation rate, used to cast the films.[25,37] In photodiodes constructed with polyfluorene derivatives, the photovoltaic quantum efficiency is also seen to be strongly dependent on the solvent evaporation rate.[4] Different morphologies, resulting in varying degrees of interchain interactions, influence the rate constant of exciton bimolecular annihilation dynamics.[25] We see evidence of the dependence of exciton decay dynamics on spin speed. Figure 7 shows transient absorption dynamics at a low pump fluence at a probe photon energy of 1.46 eV, for the thin ($\sim$30 nm) and thicker ($\sim$100 nm) films used in this study. The thinner film displays an increased decay rate, also evident at a probe photon energy of 2.70 eV (not shown here). A similar but less marked trend is observed for F8BT samples. Comparison of absorption transients of a $\sim$100-nm-thick film with those of a drop-cast film reveals that the dynamics of the latter (lower solvent evaporation rate during casting) shows slower average dynamics. We attribute this to different degrees of interchain interactions, resulting from using different solvent evaporation rates during film preparation. Bearing this in mind, we note that the purpose of this work is to explore competing exciton dissociation pathways, and to correlate these with the specific chemical composition. Although the *rate* of exciton bimolecular annihilation, for example, is dependent on interchain packing, the *mechanism* is not.

The behavior of the initial $\Delta T/T$ signals for the PA and SE bands is shown in Fig. 8(a). The values of $\Delta T/T$ at t

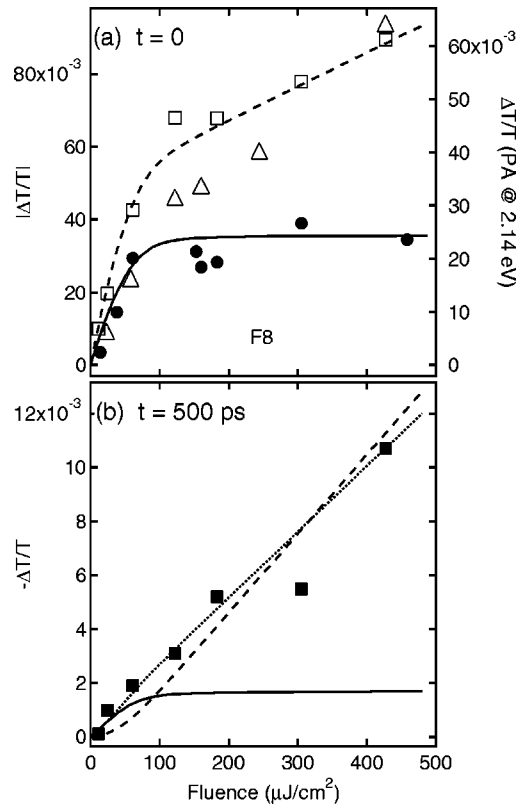

FIG. 8. Measured and simulated fluence dependence of $\Delta T/T$ signals for F8. (a) shows the measured $\Delta T/T$ signals at $t=0$ for the SE (filled circles), the PA at 2.14 eV (triangles), and the PA at 1.46 eV (open squares). Note that the PA at 2.14 eV uses a right side axis. The solid line shows the simulated SE, while the dashed line shows the simulated PA at 1.46 eV (contributions from excitons and charges generated by sequential excitation). (b) shows the PA at 1.46 eV measured at 500 ps after excitation (filled squares). The predictions of the model are shown for the cases where the charge population contains contributions from only exciton-exciton annihilation (solid line), only sequential excitation (dashed line), and a linear combination of both (dotted line).

$=0$ were obtained by fitting the measured dynamics in the range -1 to 5 ps with a double-exponential function convolved with the instrument response function, and then extrapolating to zero time. 100-nm-thick films (which show line narrowing) were used to obtain the data shown in Fig. 8, because the signal-to-noise ratio was better in the thicker films. However, comparison with data from thin films showed that line narrowing had no effect on the initial $\Delta T/T$ fluence dependence.

The magnitude of the $t=0$ SE signal from F8 saturates at a fluence of $\sim 100\ \mu J/cm^2$, while the initial signal of both PA bands continues to grow at all fluences. As modeled later, the SE signal saturates because the ground-state population is depleted at high pump fluences. The observed saturation fluence (Φ_{sat}) is consistent with the ground-state absorption cross section (i.e., $\sigma_{gs}^{-1} \Leftrightarrow \Phi_{sat}$). The magnitude of the near-IR PA band (which is known to have a contribution from excitons[11]) continues to increase above the ground-state saturation fluence as a result of a secondary species. The growth of this additional species is instrument limited (faster than 150 fs). Furthermore, it must be created from an intermediate state rather than being excited directly from the ground state. If it were created by direct excitation, then it would show the same saturation behavior as the exciton signal, and so would not increase in magnitude above the exciton saturation fluence.

Another possible explanation for the differences in saturation fluence of the initial SE and near-IR PA is that the latter contains significant contributions from direct excitation of aggregate species, which have distinctly redshifted absorption and emission spectra relative to the single-chain conjugated backbone. The absorption cross section of the aggregate transition is expected to be different than the single-chain transition, leading to a different saturation fluence. We do not consider that this is the case by comparison of the saturation data of two different F8 films with contrasting morphology. A film that was thermally annealed above the liquid crystalline transition temperature for several hours, and then rapidly quenched by placing it on a cold metallic heat sink, which was shown to retain the morphology of the liquid-crystalline phase,[5] showed no significant difference in saturation behavior than as-spun films.[38] However, the root-mean-square film roughnesses, as determined by atomic force microscopy, were 1.6 and 0.36 nm, respectively. This suggests that the difference in saturation fluences between SE and PA is not dependent on the degree of aggregation. A similar conclusion can be drawn from related measurements on polyindenofluorene derivatives containing different side

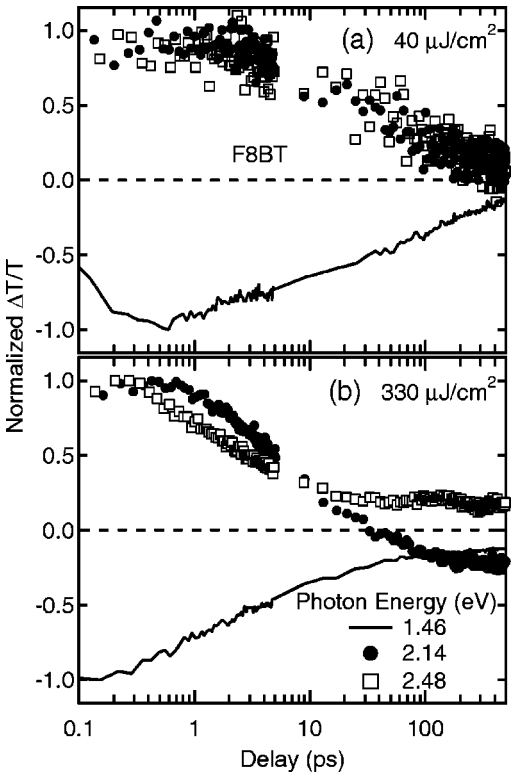

FIG. 9. Normalized transient absorption dynamics of F8BT. (a) shows the dynamics at a low pump fluence, and (b) the dynamics at a high fluence. The legend indicating the photon energy for both panels is shown in (b).

groups.[10,28] One derivative, containing linear alkyl side groups, shows a very rough surface topography, accompanied by a dominant redshifted emission feature. Another derivative, with bulky side chains, displays a significantly smoother topography and shows no such aggregate PL features. The saturation fluence of the analogous initial SE and PA shows no marked difference for the two derivatives.

The magnitude of the 1.46 eV PA signal from F8 measured 500 ps after pumping is shown by the filled squares in Fig. 8(b) as a function of the pumping fluence. At this long delay there should be no contribution to the signal from excitons. This graph therefore displays the fluence dependence of the promptly generated but long-lived species in F8.

2. F8BT

The measured transient absorption dynamics of F8BT are shown in Fig. 9. At a low pump fluence, the PA at 1.46 eV (solid line), the SE at 2.14 eV (filled circles), and the bleach signal at 2.48 eV (open squares) all have the same decay dynamics, indicating that the only species present is the singlet exciton. As with F8, the dynamics become more complicated at a high pump fluence. With a pump fluence of $\sim 330\ \mu J/cm^2$, the PA at 1.46 eV and the bleach both have an initial fast decay followed by a very long-lived tail. The bleach and the near-IR PA have very similar dynamics over the whole time range. The bleach and PA signals can be explained as arising from a fast decay due to excitons and a very slow decay due to polarons. Since no spectral line narrowing is observed in these F8BT samples, the fast initial decay of PA and bleach signals must be due to other exciton decay routes. We show below that exciton-exciton annihilation can explain the fast early-time dynamics.

For a high pump fluence, the dynamics at 2.14 eV show an initial stimulated emission signal which becomes net PA after a few tens of picoseconds. The exact time at which the zero crossing occurs depends sensitively on the pump fluence. The rapid gain depletion to net loss at this pump fluence explains why no spectral line narrowing is observed in this sample. We note that although the SE signal has a fast decay component at high pump fluences, it is not as fast as that seen in the bleach or PA dynamics at comparable pump powers. As described in more detail below, this discrepancy might be explained by the presence of an underlying PA band at the same spectral position as the SE. We presume that this band has the same origin as the visible PA band which occurs in F8, although we cannot confidently assign it to a particular species.

The initial $\Delta T/T$ signals for F8BT are shown in Figs. 10(a) and 10(b). No saturation of either the bleach or the PA occurs for any pump fluence, indicating that no saturation of the ground state occurs in F8BT within the fluence range used here. Rather, the signals grow linearly with the fluence, and point toward a larger ground-state population density in F8BT and a smaller ground-state absorption cross section at the pump wavelength. The magnitude of the 1.46-eV PA signal from F8BT, measured 500 ps after pumping, is shown by the filled squares in Fig. 10(c) as a function of the pumping fluence. As in F8, the magnitude of the long-lived component grows linearly with the pump fluence.

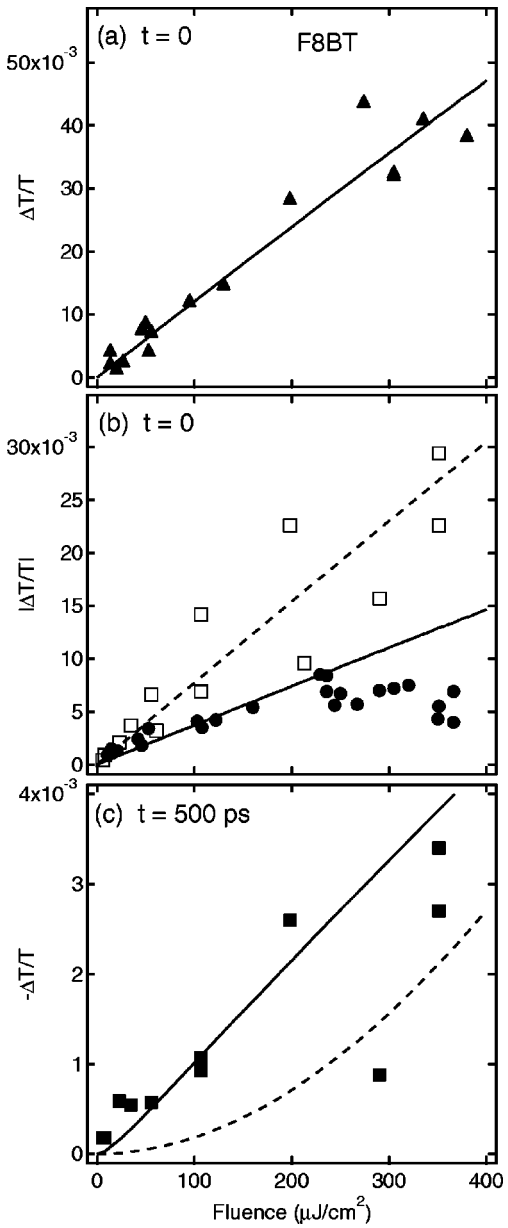

FIG. 10. Measured and simulated fluence dependences of $\Delta T/T$ signals for F8BT. (a) shows the $t=0$ $\Delta T/T$ signal of the bleach measured at 2.48 eV (triangles), and the simulated fluence dependence for $N_{gs}=4\times10^{20}\ cm^{-3}$. (b) shows the $t=0$ magnitude of the SE at 2.14 eV (circles), and the near-IR PA at 1.46 eV (open squares), along with the simulated fluence dependence of the PA (dashed line) and SE (solid line). (c) shows the near-IR PA measured at 500 ps after excitation (filled squares). The simulated fluence dependence at this delay is shown for cases where the long-lived component of the PA is caused by charges which are generated via exciton-exciton annihilation (solid line) or sequential excitation (dashed line).

IV. ANALYSIS AND DISCUSSION

A. Assignment of the observed photoinduced features

In accord with previous studies on π-conjugated oligomers[17] and related conjugated polymers,[11,16] it is clear that singlet excitons are predominantly responsible for the

PA band peaked at 1.5 eV in both F8 and F8BT when a low pump fluence is used. At a high fluence, the observation of a very long-lived component in the PA dynamics indicates that another species is present that has an absorption overlapped with that of the singlet exciton. Long-lived species which give rise to broad PA signals in the near-IR and visible have also been observed in other conjugated polymers.[13,39] We suggest that these species arise from exciton-exciton annihilation and sequential excitation, and consist of radical ions (polarons). With the aid of the photophysical model, we discuss the charge generation mechanisms in more detail below.

The long-lived near-IR PA band is formed too quickly to be the result of triplet excitons formed by intersystem crossing, which in conjugated polymers has been observed to occur on time scales of hundreds of picoseconds to nanoseconds.[40–42] The possibility of subpicosecond triplet formation by singlet fission (during exciton thermalization) has been proposed to occur when high-lying excitons are created using high-energy photons.[43] However, the number of triplets formed by this mechanism depends linearly on the ground-state population density. The triplet population should therefore have the same saturation behavior as the exciton population. As shown in Fig. 8(b), the magnitude of the long-lived component in F8 continues to grow even though the exciton population is saturated, therefore ruling out this process of rapid triplet generation by direct excitation. However, we have demonstrated that sequential excitation, first to the lowest singlet exciton, then to a high-energy exciton, is possible in the fluence range of these experiments in polyindenofluorene derivatives;[28] and singlet fission to produce triplet states is possible by this mechanism and not ruled out herein. However, the spectral position and width of the near-IR band at long pump-probe delay is inconsistent with triplet-induced absorption characterized by quasi-steady-state photoinduced absorption spectroscopy.[44]

Kraabel *et al.*[11] assigned the visible PA band to polarons. In a pristine polymer the formation mechanism is suggested to be similar to that proposed for interchain excitons in oligomers, namely, the decay of a biexciton which is formed by sequential excitation. Experiments by Klimov *et al.*, comparing the transient absorption of films and solutions of a conjugated oligomer, found that the visible PA, which is present in films, is absent in solutions.[17,45] This led these authors to conclude that the species responsible for the visible PA is an interchain exciton. We do not consider that interchain excitons are likely to be formed with such a high yield and so promptly, since this species is expected to be extrinsically stabilized, and population of these states would be limited by the relaxation rate of intrachain excitons, which we expect would occur in time scales longer than our instrument resolution. We favor the assignment of Kraabel *et al.*

Using quasi-steady-state photoinduced absorption measurements on F8, Cadby *et al.*[44] demonstrated polaron absorption peaked near 2 eV. A visible PA band was also been observed in ladder-type poly-*p*-phenylene (LPPP),[46] and assigned to charged species. In related measurements on a polyindenofluorene derivative, which is an intermediate member of the step-ladder polymer family between polyfluorene and L-PPP, we have identified a polaron peak near 2 eV.[28] If charge imbalance arises due to some electron loss mechanism, and oppositely charged radical ions have different absorbtion spectra, the visible PA band in F8 might also be caused by charges, in particular, negative polarons. It was recently shown by Wegewijs *et al.* that electrons can be emitted from conjugated polymer films under exposure to intense optical excitation.[47] This might occur if sequential excitation gives an electron energy greater than the vacuum level, so that it can escape from the material. The charge imbalance caused by photoejection of electrons from F8 might therefore explain the observed behavior of the visible PA band. The negative polarons which remain in the material after sequential excitation (and subsequent ejection of some electrons) could rapidly recombine with the larger population of positive polarons. If the visible PA band is caused by negative polarons, a relatively fast decay of this band would then be observed. Correspondingly, the population of positive polarons, which in this scenario are responsible for the near-IR PA, would be long lived because of a lack of oppositely charged species with which to recombine.

This scenario is feasible in F8, where the vacuum level is accessible in a two-step process involving, first, the creation of a singlet $1B_u$ exciton, and then the absorption of a 3.18-eV pump photon. However in F8BT, the ground-state and $1B_u$ energies are lower than in F8, meaning that sequential excitation would be less likely to give an electron sufficient energy to escape from the polymer.

B. Photophysical modeling

Several recent studies reported comprehensive photophysical modeling by solution of the relevant rate equations.[32,33,48,49] The focus of these studies was on understanding the line-narrowing mechanism and the corresponding rapid exciton depopulation. The results which were obtained added further weight to the arguments in favor of the ASE as the line-narrowing mechanism. The emphasis here is on exciton relaxation pathways other than the ASE, in particular the processes of exciton-exciton annihilation and sequential excitation.

The model developed here used a set of nodes defined by a cylindrical polar coordinate system. The exciton and charge densities at each node were calculated using the Runge-Kutta method to approximate the solution of the rate equations at a discrete set of times. The excitation pulse was taken to have Gaussian profiles in both time and space. The exciton generation at each node was calculated from the number of pump photons at that node and the probability of absorption. The pump photon flux at depth was calculated from the known photon flux at the surface and the absorption coefficient, including ground-state saturation effects.

The exciton decay mechanisms included in the present model were natural exciton decay, sequential excitation, and exciton-exciton annihilation through diffusional collision and Förster energy-transfer mechanisms. With the exception of natural exciton decay, it was assumed possible that each of these processes could produce charges.

In this section we present rate equations which describe the exciton decay and charge generation mechanisms operat-

ing in conjugated polymers. A brief explanation of each of the terms is given here. Full details of the development of these equations can be found in the Appendix.

The rate equation describing the population density of excitons, N, is

$$\frac{dN}{dt} = W(N,t) - \frac{N}{\tau} - \beta N^2 - (2-\eta)k_F(N)N - \sigma_{seq}P(t)N. \quad (1)$$

$W(N,t)$ is the rate of exciton creation by the pump pulse. We stress that the rate of exciton creation is not necessarily linearly dependent on pump fluence. Its value depends on the exciton population already present, because we have taken the finite ground-state density into account when calculating $W(N,t)$. Indeed, the saturation of the excited-state population which occurs in F8 is one of the principal reasons for the nonlinear response of that material. N/τ describes the unimolecular exciton decay rate, and includes both radiative and nonradiative components; τ is the observed PL lifetime at a low pump energy (i.e., in the absence of nonlinear exciton decay routes). For F8 we used $\tau = 120$ ps,[50] while for F8BT we used $\tau = 485$ ps.[51] βN^2 accounts for exciton loss through diffusion-limited exciton-exciton annihilation; β is the annihilation rate constant. Exciton-exciton annihilation by Förster interaction is included through the term $(2-\eta)k_F(N)N$, where η accounts for the fraction of highly excited states created by annihilation which relax back to singlet excitons (rather than dissociating into charges), and $k_F(N)$ is the Förster annihilation rate constant. The term ''rate constant'' is used loosely in this case, because k_F depends explicitly on the exciton density, and hence implicitly on time. This comes about because of the strength of the Förster interaction depends on the exciton separation, which is in turn related to the exciton density. Full details of the exciton density dependence of k_F can be found in the Appendix. Exciton loss through sequential excitation is described by $\sigma_{seq}P(t)N$, where σ_{seq} is the effective cross section for charge generation and $P(t)$ is the pump photon flux. σ_{seq} is a compound cross section which includes the cross section for absorption by the excited state and the fraction of sequentially excited states which dissociate to form charges. As in our previous work,[28] we assume that the sequentially excited state either rapidly dissociates or rapidly relaxes back to the lowest singlet level.

If it is assumed that all of the exciton decay mechanisms except unimolecular decay can produce charges, the rate equation describing the population density of charge pairs, N_c, is,

$$\frac{dN_c}{dt} = \frac{1-\eta}{2-\eta}\beta N^2 + (1-\eta)k_F N + \sigma_{seq}P(t)N - \frac{N_c}{\tau_c}. \quad (2)$$

In all the simulations performed here the lifetime of the charges, τ_c, is taken to be 2 ns, as indicated by multiexponential fits to the near-IR PA transients. This decay constant only serves to model the slow decay, and should not be taken to mean that the charges actually have a well-defined lifetime. Indeed, experiments have shown that the charges in conjugated polymers have a wide range of lifetimes (extending into the ms range), possibly because of the inhomogeneous environment.[52,53] Of more interest in the present calculations is the lifetime of the excitons and the rate of creation of charges via exciton decay.

TABLE I. Summary of parameters used in the modeling of the dynamics for F8 and F8BT.

	F8	F8BT
N_{gs} (cm^{-3})	2×10^{19}	4×10^{20}
β (cm^3 ps^{-1})	2.5×10^{-20}	1.5×10^{-21}
γ (cm^3 ps^{-1})	4.9×10^{-20}	2.6×10^{-21}
η	1	0.85
R_0 (nm)	–	4
σ_{gs} (cm^2)[a]	1.3×10^{-14}	9.5×10^{-17}
σ_{seq} (cm^2)	4×10^{-16}	0

[a]Ground-state absorption cross section at pump photon energy (3.18 eV).

Although Eq. (1) contains four terms describing the decay of the exciton population, the only freely adjustable parameters which affect the decay rate are k_F and η. The value of τ is set from time-resolved PL measurements, β is set by fitting the integrated PL data, and σ_{seq} can only affect the dynamics during the pump pulse. Furthermore, since η can only take on values between 0 and 1, it can at most change the rate of decay due to Förster interaction by a factor of 2. Therefore, the dynamics during the first few picoseconds after excitation are most strongly determined by the value of k_F.

There are several parameters which can be simultaneously varied in order to fit the data. The procedure which was used to acquire the parameters was the same for F8 and F8BT. First the ground-state density was estimated as discussed below; then the diffusion-limited annihilation rate constant was determined, the effectiveness of sequential excitation was deduced, and finally the extent of exciton-exciton annihilation by the Förster mechanism was found. In all cases, determination of the parameters was made by graphical comparison of the experimental results and those of the model. A summary of the parameters is shown in Table I.

1. F8

In F8, the ground-state density N_{gs} was estimated by fitting the saturation of the $t=0$ stimulated emission data, and also by fitting the measured amount of pump light transmitted through the sample as a function of pumping intensity. When using either method, the model could fit the data with $N_{gs} = 2\times10^{19}$ cm^{-3}. The simulated $t=0$ $\Delta T/T$ signal for the SE from F8 is shown by the solid line in Fig. 8(a). The simulated transmission of the pump through a film of F8 is shown by the solid line in Fig. 3(a), and is compared to the measured transmission. As defined here, the ground-state density is the maximum number density of excitons which can be formed in the polymer.

The model could fit the integrated PL data for F8 (result in Fig. 2) when $\beta = 2.5\times10^{-20}$ cm^3 ps^{-1}. The dashed lines

in Fig. 2 show the effect of turning off exciton-exciton annihilation. The slight turnover at high pulse energy in the curve for F8 is due to a saturation of the ground state. The exciton diffusion coefficient, as defined in the Appendix [Eq. (A4)], is calculated to be $D=2\times10^{-2}$ cm^2 s^{-1} for F8 (assuming $R_e=1$ nm). Typical values of the exciton diffusion constant in other conjugated polymers range from $D\approx1\times10^{-4}$ cm^2 s^{-1} (Refs. 54 and 55) for PPV and its derivatives, to 4.4×10^{-2} cm^{2}s^{-1} (Ref. 56) for L-PPP. A value of $D\approx1\times10^{-2}$ cm^{2}s^{-1} can be inferred from our previously published data for a polyindenofluorene derivative.[10] It is interesting to note that the diffusion constant found for F8 is consistent with the values for other members of the family of step-ladder polymers which are based on PPP.

The initial $\Delta T/T$ data in Fig. 8(a) show that the SE signal saturates, while the PA at 1.46 eV does not. Charges produced by exciton-exciton annihilation[24] cannot be the cause of this promptly generated absorbing species, since they would not be formed fast enough to make a significant contribution at $t=0$. Within the framework of the model described here, sequential excitation leads to a rapid formation of charges which, in conjunction with exciton absorption, give rise to the near-IR PA at $t=0$. The contribution that charges make to the magnitude of the initial PA signal depends on the number of charges which are created (determined by the effective cross section for charge generation, σ_{seq}) and the absorption cross section of the charges. Because these are independent parameters, it was not possible to obtain unique values for each of them. However, charges in LPPP, which is in the same family of step-ladder polymers as F8, have been found to have an absorption cross section of 4×10^{-16} cm^2.[56] If the same value is assumed for the charges in F8, the effective cross section for charge formation by sequential excitation needs to be $\sigma_{seq}=4\times10^{-16}$ cm^2 in order to fit the data given the charge population calculated with Eq. (2). Such a fit to the initial 1.46-eV PA data is shown by the dashed line in Fig. 8(a). It is interesting to consider the threshold of exciton dissociation by sequential excitation. From the modeled initial $\Delta T/T$ at 1.46 eV [Fig. 8(b)], an inflection point is observed at 100 μJ/cm^2. Below this fluence, the dependence is linear, indicating that singlet exciton absorption is the primary contributor to the signal. Above this fluence, the simulated dependence is also linear, but with a different slope, due to the linear growth of polaron pairs. The threshold for the sequential step is thus close to the inflection point.

The fact that the initial $\Delta T/T$ PA at 1.46 eV continues to increase in magnitude, even when the ground state has been saturated, shows that an intermediate species is involved in the generation of charges. Although formation of charges by direct excitation from the ground state can explain their rapid appearance,[27] it cannot explain why the charge population continues to increase even above the saturation fluence. It can be argued that the SE saturation may be alternatively caused by a decrease in gain resulting from the additional transient absorption from polarons, which have absorption tails extending into the gain region. However, the PA band would require the precisely correct fluence dependence to cancel the increasing SE and result in apparent saturation, which is unlikely. Also, the saturation fluence in Fig. 8 is consistent with the ground-state absorption cross section.

All the zero-time data for F8 in Fig. 8(a) were fit by assuming that sequential excitation was the only operative charge generation mechanism. Although it may be possible for exciton-exciton annihilation to generate charges,[24] these would not be present at $t=0$. Adequate fits to the data were obtained by assuming that exciton-exciton annihilation produced no charges in F8 (i.e., setting $\eta=1$).

The high value of β is found by fitting the model to the integrated PL data results in strongly intensity-dependent dynamics, with fast decay at early times. Förster annihilation was not needed in order to reproduce the dynamics observed for F8. Indeed, as shown below, Förster annihilation is not expected to be significant in F8 because the PL spectrum is sufficiently blueshifted from the exciton absorption so that the spectral overlap, and hence k_F, is negligibly small. Therefore, the dynamics for F8 could be adequately simulated by using diffusion-limited annihilation as the dominant exciton depopulation mechanism. Results of the simulation for a variety of pump fluences are shown by solid lines in Figs. 6(a) and 6(b), and are compared to the measured dynamics. We note that although the rate constant of exciton bimolecular annihilation is sensitive to the preparation procedure,[25] the dynamics cannot be fit successfully invoking a Förster mechanism.

An argument which has been put forward against the diffusion-limited annihilation mechanism is the expectation that the exciton decay rate will increase without limit as the pump fluence increases.[17] However, when saturation of the ground-state population is taken into account, we find that there is an upper limit on the exciton density, and consequently an upper limit on the bimolecular decay rate.

Figure 8(b) shows that the magnitude of the PA at a delay of 500 ps, which is due solely to charges, grows linearly with increasing fluence. This behavior can be reproduced with the model if sequential excitation is the sole cause of charge generation. However, we also note that a linear combination of charges generated by sequential excitation and exciton-exciton annihilation fits the data at these long delays slightly better. Because the exciton population saturates at high fluences, the number of charges formed through annihilation alone also saturates [shown by the solid line in Fig. 8(b)], adding further weight to the argument in favor of sequential excitation as the dominant charge generation mechanism.

2. F8BT

For F8BT, the ground-state density was found by fitting the model to the $t=0$ bleach signal for a range of pump fluences. The bleach signal at a particular wavelength is given by

$$\frac{\Delta T}{T}=\exp\left(\alpha z\frac{N_{exc}}{N_{gs}}\right)-1, \tag{3}$$

where α is the linear absorption coefficient at that wavelength, $N_{exc}=N+N_c$ is the total number of chromophores removed from the ground state by the pump, and z is the film thickness. N_{gs} was varied until the correct fluence depen-

dence of $\Delta T/T$ was reproduced. The result of the fitting for $N_{gs}=4\times10^{20}$ cm^{-3} is shown by the solid line in Fig. 10(a). This value of N_{gs} is a factor of 20 higher than the value for F8, but is supported by the observation that no saturation of the $\Delta T/T$ signal occurs even for the highest values of N_{exc} used in these experiments ($>2\times10^{19}$ cm^{-3}). A further and independent confirmation of a large ground-state density in F8BT is provided by the observation of a linear dependence of the amount of pump light transmitted through F8BT films, as shown in Fig. 3(b).

The diffusion-limited annihilation rate constant β was found by fitting the model to the integrated PL data shown in Fig. 2. The integrated PL is a useful indicator of β, since diffusion-limited annihilation occurs at relatively low pulse energies, when annihilation by Förster transfer can be ignored. As described in the Appendix, Förster annihilation only occurs at early times after intense pumping, when the mean exciton separation is sufficiently small. On the other hand, diffusion-limited annihilation will tend to have a significant effect on the integrated PL over longer time periods, during which the excitons will have sufficient time to ''find'' each other by diffusion.

The results of modeling the integrated PL from F8BT are shown in Fig. 2. Both diffusion-limited and Förster annihilation were included in the fit, and the combination of the two slightly underestimates the PL intensity at the highest fluences. However, Förster annihilation on its own was unable to reproduce the PL intensity data, and diffusion-limited annihilation alone cannot explain the fast exciton decay at short times after excitation. Therefore, a combination of both mechanisms is believed to operate in F8BT at high pump intensities. The value of β which best fits the integrated PL data at a low pump energy (when Förster annihilation is unimportant) is 1.5×10^{-21} cm^3 ps^{-1}. Equation (A4) then shows that the exciton diffusion coefficient in F8BT is $D=2.6\times10^{-4}$ cm^2 s^{-1} (assuming $R_e=4$ nm, as discussed below). We note that the extracted diffusion coefficient in F8BT is significantly smaller than in F8, perhaps pointing to F8BT having a more disordered structure.

The dynamics of the ground-state bleach in F8BT at a high pump intensity, shown in Fig. 9(b), indicate that a significant fraction of the population remains excited on a nanosecond time scale. In order to fit this slow ground-state recovery it is necessary to have a significant fraction of the excitons decay into long-lived charges. This can occur either if sequential excitation is strong, or if η is less than unity. Fitting the long-time bleach dynamics shows that if sequential excitation alone is responsible for the large charge population, then a value of the sequential excitation cross section needs to be of the order $\sigma_{seq}=3\times10^{-16}$ cm^2. However, this value is large compared to the cross section for ground-state absorption at the pump wavelength, which is $\sigma_{gs}=9.5\times10^{-17}$ cm^2. As discussed in the Appendix, such a large sequential excitation cross section seems unlikely, since it would preclude the observation of a ground-state bleach.

Further evidence that sequential excitation is not the dominant charge generation mechanism in F8BT comes from the linear fluence dependence of the 500-ps charge population [Fig. 10(c)]. If sequential excitation is the principal charge generation mechanism, then a quadratic dependence on pump fluence would be expected if the lowest singlet exciton population density is not saturated, as shown by the dashed line. We have strong evidence of a linear excitation density in the range of pump fluences used in the experiment, ruling out sequential excitation as an important source of charge density in F8BT.

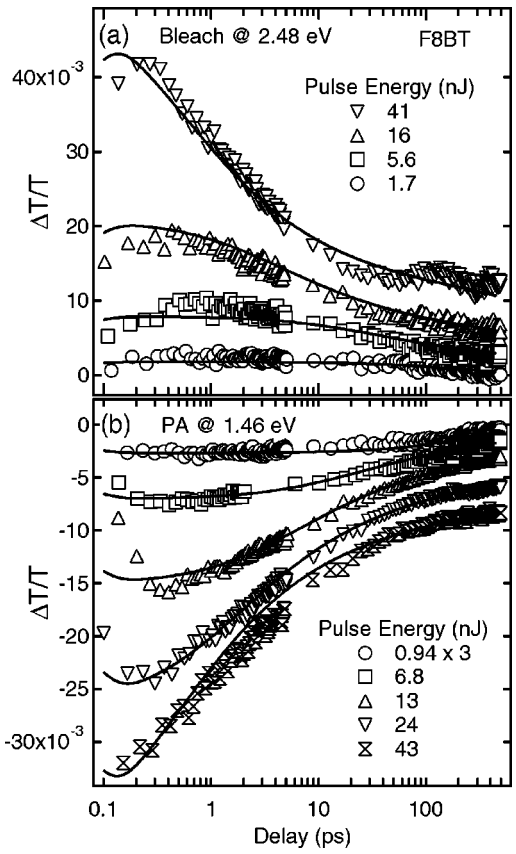

FIG. 11. Transient absorption dynamics of the bleach (a) and near-IR PA (b) from F8BT at a range of pump energies. In each case, the results of the model are shown as solid lines. Traces have been offset for clarity.

On the other hand, if sequential excitation is turned off by setting $\sigma_{seq}=0$, the model predicts that the charge population generated by Förster annihilation will be linearly dependent on the fluence, in agreement with observation. It is found that a value of $\eta=0.85$ gives the observed fraction of excitons decaying to long-lived charges. The values of $\eta=0.85$ and $\sigma_{seq}=0$ are used for the rest of the fitting of F8BT data.

Using the parameters found so far, the dynamics of the PA at 1.46 eV and the bleach at 2.48 eV were fit by varying the critical distance for Förster interaction, R_0. It was found that $R_0=4$ nm gave good fits to all the data, as can be seen in Fig. 11. This value of R_0 compares favorably with the value calculated using Förster theory (see below).

For F8BT at high pump fluences, the SE dynamics and the fluence dependence of the $t=0$ SE magnitude were not well reproduced with the model in its current form. The fast decay component which is observed in the photoinduced absorption and the bleach at high pump fluences [Fig. 9(b)] is

well reproduced using the model. However, this fast decay is absent from the SE dynamics. Furthermore, the initial magnitude of the SE [Fig. 10(b)] is unexpectedly small, and grows nonlinearly with the fluence. This is surprising because the exciton population is known to grow linearly with the fluence, as is made evident from the linear growth of the near-IR PA and the bleach signals. Also, the simulated fluence of the SE magnitude grows linearly, since this assumes a linear fluence dependence of the exciton population.

A possible explanation for these discrepancies is that the species which leads to the visible PA band in F8 is also present in F8BT, and contributes to the $\Delta T/T$ signal measured at 2.14 eV. The presence of this underlying PA, which in F8 has a fast decay component, would lead to the net measured SE being relatively slowly decaying and small in magnitude. We have suggested that this species is one of the decay products of the sequentially excited state. In F8BT, where no saturation of the ground state occurs, the population of this species would be expected to grow quadratically with pump fluence. The quadratic growth of an underlying PA would also explain the nonlinear growth of the $t=0$ SE signal shown in Fig. 10(b). By including a negative contribution with a quadratic fluence dependence in the overall SE, we were able to reproduce the measured SE dynamics (not shown here).

3. Direct calculation of R_0 for F8BT

The value of the critical distance for Förster interaction R_0 can be calculated from the equation

$$R_0^6=\frac{9000(\ln 10)\kappa^2}{128\pi^5 n^4 N_{Av}}c^4\int_0^\infty \frac{f_D(\nu)\varepsilon_A(\nu)}{\nu^4}d\nu, \tag{4}$$

where n is the refractive index of the medium between donor and acceptor, N_{Av} is Avogadro's constant, c is the speed of light, and κ^2 is the orientation factor. The integral accounts for the spectral overlap of the donor emission spectrum $[f_D(\nu)]$, normalized so that $\int_0^\infty f_D(\nu)d\nu=1$, and the acceptor absorption spectrum represented by the molar extinction coefficient, $\varepsilon_A(\nu)$.

Note that, as described in the Appendix, we have defined the Förster rate in terms of the *natural radiative lifetime* of the donor (rather than the PL lifetime). Therefore, the donor quantum yield, which usually appears in the numerator of Eq. (4), is already accounted for and does not appear here.

Equation (4) shows that in order to have an appreciable interaction, the donor emission spectrum must overlap with the acceptor absorption. In exciton-exciton annihilation, excitons act as both donors and acceptors, so annihilation via Förster transfer requires an overlap between the PL spectrum and the exciton absorption. F8BT has a PL spectrum which is significantly redshifted relative to that of F8, while the exciton absorption spectra in the two materials appear similar. Consequently there is much more overlap of exciton absorption and emission spectra in F8BT than occurs in F8.

R_0 was calculated for F8BT. The exciton absorption spectrum was extracted from the 1-ps low fluence $\Delta T/T$ spectrum shown in Fig. 5(a). This was achieved by removing the contribution from stimulated emission to the overall transient absorption spectrum. In doing this, it was assumed that the shape of the SE spectrum was the same as the PL spectrum. The PL spectrum was scaled so that it was the same magnitude as the SE at 2.3 eV, then subtracted from the $\Delta T/T$ spectrum. This assumes that the exciton absorption at 2.3 eV is zero, which may not be the case. It is therefore expected that this procedure will slightly underestimate the amount of spectral overlap. However, the error should not affect the calculated value of R_0 very strongly, because taking the sixth root of the overlap integral means that large changes are required in order to affect R_0. The exciton absorption cross section σ was calculated using

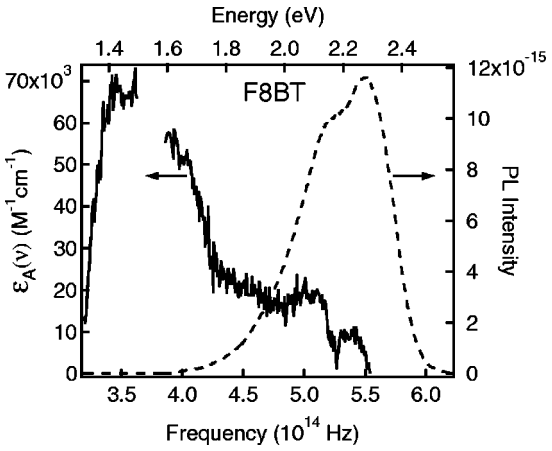

FIG. 12. The molar absorption coefficient of excitons, $\varepsilon_A(\nu)$, and the normalized PL emission spectrum as functions of frequency ν for F8BT.

$$\sigma(\nu)=-\frac{1}{Nz}\ln\left(1+\frac{\Delta T}{T}(\nu)\right), \tag{5}$$

where z is the film thickness. Once $\sigma(\nu)$ is known, the molar absorption coefficient can be found using[57]

$$\varepsilon(\nu)=\frac{\log_{10}e}{1000}N_{Av}\sigma(\nu). \tag{6}$$

$\varepsilon(\nu)$ and the normalized PL spectrum of F8BT are shown in Fig. 12. Evaluating the integral in Eq. (4) and using $n=1.8$ (measured using ellipsometry) and $\kappa^2=0.655$ (appropriate for the case where the donor and emitter dipoles lie in the plane of the film) gave $R_0=4.0\pm0.4$ nm. Repeating the calculation using the 1-ps high-fluence spectrum yielded $R_0=4.2\pm0.4$ nm.

The distances calculated here are close to the value of $R_0=4.5$ nm found by Dogariu *et al.*[23] for exciton-exciton annihilation in a dialkoxy-substituted PPV derivative. Those authors used this value to infer a highly delocalized exciton. They argued that because annihilation occurs when the mean exciton separation is 10 nm, dipole-dipole interaction (over 4.5 nm) and exciton diffusion (over <1 nm) cannot explain the interaction which occurs during the first few picoseconds after excitation. However, their calculations were based on the *mean* exciton separation. This overlooked the fact that many of the excitons created in a disordered polymer film

will be considerably closer than the mean separation. We propose that it is these near neighbors which interact via the Förster mechanism in the first few picoseconds after excitation, and give rise to the fast initial decay. Indeed, it is the fast depletion of the near neighbors which leads to the time dependence of the rate constant k_F which is empirically represented by $1/\sqrt{t}$. We therefore do not believe that highly delocalized excitons are necessary to explain our results.

V. CONCLUSIONS

In summary, we have performed time-resolved measurements of the excited-state absorption in thin films of the polyfluorene derivatives F8 and F8BT. Using a detailed photophysical model, we have investigated the mechanisms which are responsible for exciton dissociation. At moderately high pumping intensities, the lifetime of the singlet excitons is dramatically decreased due to depopulation by exciton bimolecular annihilation.

In contrast to previous studies of exciton-exciton annihilation, which discussed only one mechanism for this process, we have shown that annihilation can proceed via two different mechanisms. The first, which dominates in F8, is a collisional process which is limited by exciton diffusion. The second, which dominates in F8BT, occurs via Förster interaction between excitons. We have shown that the strength of the Förster mechanism depends on the extent of the overlap between exciton emission and absorption spectra, and therefore is strongest in polymers with long wavelength emission, notably alkoxy-substituted PPV derivatives. We do not believe that a spatially delocalized exciton wave function[23] is required to explain our results.

We suggest that polaron pairs are responsible for the very broad and long-lived PA band which is apparent at higher pumping fluences. We show that these can be formed by two different mechanisms. In F8, sequential excitation leads to charges being produced only during the pump pulse and these can contribute to the initial transient absorption signal. In contrast, the near-IR PA in F8BT comes from charges which are thought to arise predominantly from exciton-exciton annihilation. This operates via the Förster mechanism, with sequential excitation making little contribution to the charge population. All our results can be explained using these two charge generation mechanisms, without recourse to the concept of direct charge generation.[27]

The conclusions regarding the mechanisms of exciton-exciton annihilation, which have been presented here, have implications relevant to the fabrication of electrically pumped polymer lasers. The usual approach to lowering the laser threshold in optically pumped devices has been to shift the laser emission to longer wavelengths in order to avoid the ground-state absorption. However, this is disadvantageous for two reasons: first, the presence of excited-state absorption at longer wavelengths (e.g., from charges and excitons) can introduce significant losses; second, the rate of exciton quenching through the Förster mechanism is increased by redshifting the laser wavelength. Our results suggest the most suitable materials for lasing are those polymers which emit in the blue part of the spectrum. Here the losses from excited-state absorption and Förster annihilation are lowest. However, it will obviously be necessary to find a trade-off between losses due to ground-state absorption and those which occur at longer wavelengths.

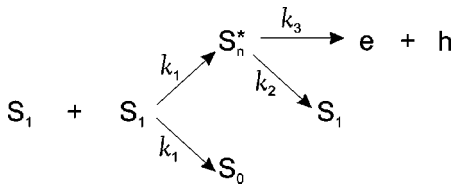

FIG. 13. Schematic of the exciton-exciton annihilation process.

ACKNOWLEDGMENTS

We are grateful to Takeo Kawase for refractive index measurements, and to Laura Herz and Dr. Richard Phillips for sharing their transient photoluminescence data prior to publication. We also thank Dr. Devin MacKenzie for performing AFM measurements on the as-spun and thermally quenched F8 samples. This research was funded by a grant from the EPSRC. M.A.S thanks the Cambridge Commonwealth Trust and the New Zealand Vice-Chancellors' Committee for financial support.

APPENDIX

This appendix contains details of how the rate equations (1) and (2) were derived. Each of the exciton-decay/charge-generation mechanisms is discussed, and the contribution to the overall rate equation is derived.

1. Exciton-exciton annihilation

Exciton-exciton annihilation has been suggested as a mechanism for depopulating the excited states in conjugated polymers.[21,24,58,59] A general scheme for exciton-exciton annihilation is shown in Fig. 13. A pair of S_1 excitons interacts with the result that one gains energy and is promoted to a higher-energy state denoted by S_n^*. The other exciton loses energy and relaxes to the ground state S_0. As discussed below, the interaction can occur either by collisionlike processes, which are limited by exciton diffusion, or by a Förster energy-transfer process.

There are two routes of decay available to the highly excited S_n^* exciton: either it can relax back to the S_1 level; or it can ionize into an electron and hole.[57] If a fraction η of the S_n^* excitons decay back to the S_1 level, then a fraction $(1-\eta)$ do not return to S_1 and so are available for generation of charges. In the simulations performed here it was assumed that as soon as S_n^* excitons are created, they either relax to S_1 or separate into charges. This means that exciton encounter is the rate-limiting step. This then allows the rate constants k_2 and k_3 to be written in terms of k_1:

$$k_2 = \eta k_1, \tag{A1}$$

$$k_3 = (1-\eta) k_1. \tag{A2}$$

It small molecules, the probability of S_n^* ionizing is quite small (i.e., η close to 1) and, when ionization does occur, geminate recombination of the electron and hole tends to reform singlet excitons.[57] However, in conjugated polymers the charges are considerably more mobile, and so geminate recombination might be less likely. Indeed, a value of $\eta \approx 0.5$ has been reported for PPV.[24]

The mechanism for exciton-exciton annihilation is a contentious issue. It was attributed to diffusion-limited processes, and also to Förster interaction. We show that both mechanisms can operate simultaneously in the materials studied here, and that the strength of the Förster interaction is determined by the overlap of the PL and exciton absorption spectra. This explains why the Förster mechanism is found in long-wavelength-emitting polymers,[22,23,25,60] while the diffusion-limited process dominates in short-wavelength-emitting polymers.[10,33,48,49]

a. Diffusion-limited annihilation

The rate of reduction of the exciton density due to the diffusion-limited exciton-exciton annihilation process is described by

$$\left(\frac{dN}{dt}\right)_{\text{dif}} = -\gamma N^2, \tag{A3}$$

where γ is the annihilation rate constant. Note that $\gamma = 2k_1$. The value of γ measures the rate of encounter of excitons, and is related to the diffusion constant D through[61]

$$\gamma = 8\pi D R_e, \tag{A4}$$

where R_e is the distance at which the interaction occurs. R_e is usually given the value of 1 nm.[61]

With reference to Fig. 13, the rate equation describing the number-density of excitons (including repopulation from the S_n^* state) is found to be

$$\begin{aligned}\left(\frac{dN}{dt}\right)_{\text{dif}} &= -\gamma N^2 + \frac{\eta}{2}\gamma N^2 \\ &= -\left(1-\frac{\eta}{2}\right)\gamma N^2 \\ &= -\beta N^2.\end{aligned} \tag{A5}$$

The observed annihilation rate-constant β can be measured by fitting the integrated PL data. From Eq. (A5), it is seen that

$$\gamma = \frac{2\beta}{2-\eta}. \tag{A6}$$

Again with reference to Fig. 13, the rate equation describing the creation of charge pairs by diffusion-limited annihilation is found to be

$$\begin{aligned}\left(\frac{dN_c}{dt}\right)_{\text{dif}} &= (1-\eta)\frac{1}{2}\gamma N^2 \\ &= \frac{1-\eta}{2-\eta}\beta N^2.\end{aligned} \tag{A7, A8}$$

b. Exciton-exciton annihilation by Förster transfer

Förster energy transfer is used to describe the interaction between an excited donor and a ground-state acceptor. Exciton-exciton interaction via Förster energy transfer was previously used to explain observations of highly intensity-dependent exciton decay dynamics.[23,62]

The rate of energy transfer between an excited donor and an unexcited acceptor is given by

$$k_F = \frac{1}{\tau_{rad}}\left(\frac{R_0}{R}\right)^6, \tag{A9}$$

where R is the distance between the donor and acceptor, τ_{rad} is the natural radiative lifetime of the donor in the absence of the acceptor, and R_0 is the critical interaction distance. R_0 is defined as the distance at which k_F is equal to the radiative decay rate. In fact, Förster defined R_0 as the distance at which k_F is equal to the sum of all the other decay rates (radiative and non-radiative).[63,64] However, this was questioned by Duysens,[65] who suggested that the form shown in Eq. (A9) is a better representation of the actual donor-acceptor interaction. The form proposed by Duysens is used here, since it avoids the ambiguity in the definition of R_0 which occurs when the nonradiative relaxation pathways have nonexponential dynamics, as occurs for sequential excitation and diffusion-limited annihilation.

When a total of N_A acceptors are present, Eq. (A9) becomes

$$k_F = \frac{1}{\tau_{rad}}\sum_{i=1}^{N_A}\left(\frac{R_0}{R_i}\right)^6. \tag{A10}$$

In order to incorporate the rate of Förster energy transfer into the rate equations for the exciton and charge populations, it is necessary to have an expression for k_F in terms of N rather than R_i. For a given exciton density N, the average exciton separation is $\overline{R} = 1/\sqrt[3]{N}$, so that $1/\overline{R^6} = N^2$. Consequently the sum $\Sigma_{i=1}^{N_A} 1/R_i^6$ is proportional to N^2:

$$\sum_{i=1}^{N_A}\frac{1}{R_i^6} = aN^2. \tag{A11}$$

The proportionality constant a was found in the following way.

A Monte Carlo simulation was performed whereby a total of N_A excitons was placed randomly throughout a small volume of space, subject only to the constraint that the exciton density in this volume was N. The volume was taken to be a cube 40 nm on a side, centered at the origin. R_i was defined as the distance from the donor exciton (located at the origin) to the ith acceptor. The dimensions of the volume were made sufficiently large so that excitons located outside it made a negligible contribution to $\Sigma_{i=1}^{N_A} 1/R_i^6$. By calculating $\Sigma_{i=1}^{N_A} 1/R_i^6$ for a range of N, the relationship between

$\Sigma_{i=1}^{N_A} 1/R_i^6$ and the exciton density was built up. By fitting Eq. (A11) to the results of the simulation, the value of $a = 8.505 \times 10^{-41}$ was determined.

Substituting Eq. (A11) into Eq. (A10) gives the rate of exciton-exciton annihilation by Förster transfer in terms of N:

$$k_F(N) = \frac{R_0^6}{\tau_{rad}} a N^2. \tag{A12}$$

The efficiency of the transfer process can be changed by adjusting the value of R_0 so as to best fit the data.

In the transfer process, the exciton which acts as the donor relaxes to the ground state, while the exciton which acts as the acceptor is raised in energy. It is assumed that the acceptor exciton is promoted to the S_n^* state, just as in diffusion-limited annihilation. Because $k_F(N)$ is defined as the rate constant for loss of excited donors, the total rate of loss of excitons (equivalent to the rate of loss of donors *and* acceptors) is *twice* the value of $k_F(N)$.

The situation is analogous to that depicted in Fig. 13, except that here the rate constants are $k_1 = k_F(N)$, $k_2 = \eta k_F(N)$, and $k_3 = (1-\eta) k_F(N)$. As before, η is the fraction of S_n^* which relax back to the S_1 level. The rate of loss of excitons through Förster annihilation is therefore

$$\left(\frac{dN}{dt}\right)_F = -2k_F(N)N + \eta k_F(N)N = -(2-\eta)k_F(N)N. \tag{A13}$$

Charge generation via Förster transfer is described by

$$\left(\frac{dN_c}{dt}\right)_F = (1-\eta)k_F(N)N. \tag{A14}$$

The rate of energy transfer depends on the exciton density and will change in time as N changes. It has been found empirically that the rate for Förster transfer can be described by a $t^{-1/2}$ dependence at times relatively far from $t=0$.[61] This explicit time dependence was recently used to model energy transfer in conjugated polymer blends[66,67] as well as the exciton-exciton annihilation process in conjugated polymers[22,23,60] and other materials.[62,68] The generally accepted interpretation of data that fits with a rate constant with $t^{-1/2}$ dependence is that such dependence arises from Förster transfer annihilation. However, the $t^{-1/2}$ dependence also arises in a phenomenological one-dimensional diffusion model.[61] We consider this to be a weakness of such a description. The data may be fit using the explicit time dependence, but it is still not possible to describe the Förster process explicitly, therefore masking the underlying physical process of Förster energy transfer. Second, it completely fails for $t \leqslant 0$, and presumably gives unphysical solutions as t approaches zero. Nevertheless, the time-dependent rate approach was used on picosecond time scales.[69] Since the aim of the present model is to describe processes on time scales less than 2 ps, including ''negative'' times (i.e., before and during the pump pulse) the use of the $t^{-1/2}$ description was not appropriate.

2. Sequential excitation

In a previous publication we described the sequential excitation process as it applies to conjugated polymers.[28] Briefly, sequential excitation occurs when an exciton is created by the pump and subsequently absorbs a second pump photon. The exciton is promoted to a highly excited state, which then either rapidly ionizes or relaxes back to the singlet exciton level. Rapid ionization of the state prepared by sequential excitation leads to charge generation only during the pump pulse duration.

The rate of exciton depopulation by sequential excitation depends both on the number of excitons present and on the number of pump photons:

$$\left(\frac{dN}{dt}\right)_{\text{seq}} = -\sigma_{seq} P(t) N. \tag{A15}$$

σ_{seq} is the effective cross-section for charge generation which includes both the cross-section for creation of a sequentially excited state and the probability that this state ionizes; $P(t)$ is the pump-photon flux. The rate of charge generation is therefore given by:

$$\left(\frac{dN_c}{dt}\right)_{\text{seq}} = \sigma_{seq} P(t) N. \tag{A16}$$

It is expected that the cross section for the sequential-excitation process will be quite small relative to the cross section for absorption into the first singlet level (σ_{gs}). This is supported by the fact that a strong ground-state bleach is universally observed in conjugated polymers at the position of the ground-state absorption. If $\sigma_{seq} > \sigma_{gs}$, a photo induced absorption would be observed instead.

Combining Eqs. (A5), (A13), and (A15) leads to Eq. (1), which is the full rate equation describing the exciton population. Similarly, Eqs. (A8), (A14), and (A16) lead to Eq. (2), the rate equation describing the charge population.

[1] M. Redecker, D.D.C. Bradley, M. Inbasekaran, W.W. Wu, and E.P. Woo, Adv. Mater. **11**, 241 (1999).

[2] M. Kreyenschmidt, G. Klaerner, T. Fuhrer, J. Ashenhurst, S. Karg, W.D. Chen, V.Y. Lee, J.C. Scott, and R.D. Miller, Macromolecules **31**, 1099 (1998).

[3] A.W. Grice, D.D.C. Bradley, M.T. Bernius, M. Inbasekaran, W.W. Wu, and E.P. Woo, Appl. Phys. Lett. **73**, 629 (1998).

[4] J.J.M. Halls, A.C. Arias, J.D. MacKenzie, M. Inbasekaran, E.P. Woo, and R.H. Friend, Adv. Mater. **12**, 498 (1999).

[5] M. Grell, D.D.C. Bradley, M. Inbasekaran, and E.P. Woo, Adv. Mater. **9**, 798 (1997).

[6] M. Grell, D.D.C. Bradley, G. Ungar, J. Hill, and K.S. Whitehead,

Macromolecules **32**, 5810 (1999).
[7] B. Schartel, V. Wachtendorf, M. Grell, D.D.C. Bradley, and M. Hennecke, Phys. Rev. B **60**, 277 (1999).
[8] M. Grell, W. Knoll, D. Lupo, A. Meisel, T. Miteva, D. Neher, H. Nothofer, U. Scherf, and A. Yasuda, Adv. Mater. **11**, 671 (1999).
[9] M. Redecker, D.D.C. Bradley, M. Inbasekaran, and E.P. Woo, Appl. Phys. Lett. **74**, 1400 (1999).
[10] C. Silva, D.M. Russell, M.A. Stevens, J.D. MacKenzie, S. Satayesh, K. Müllen, and R.H. Friend, Chem. Phys. Lett. **319**, 494 (2000).
[11] B. Kraabel, V.I. Klimov, R. Kohlman, S. Xu, H.-L. Wang, and D.W. McBranch, Phys. Rev. B **61**, 8501 (2000).
[12] W. Graupner, G. Leising, G. Lanzani, M. Nisoli, S. De Silvestri, and U. Scherf, Chem. Phys. Lett. **246**, 95 (1995).
[13] M. Yan, L.J. Rothberg, E.W. Kwock, and T.M. Miller, Phys. Rev. Lett. **75**, 1992 (1995).
[14] G.J. Denton, N. Tessler, N.T. Harrison, and R.H. Friend, Phys. Rev. Lett. **78**, 733 (1997).
[15] B. Schweitzer, G. Wegmann, H. Giessen, D. Hertel, H. Bässler, R.F. Mahrt, U. Scherf, and K. Müllen, Appl. Phys. Lett. **72**, 2933 (1998).
[16] D.W. McBranch, B. Kraabel, S. Xu, R.S. Kohlman, V.I. Klimov, D.D.C. Bradley, B.R. Hsieh, and M. Rubner, Synth. Met. **101**, 291 (1999).
[17] V.I. Klimov, D.W. McBranch, N.N. Barashkov, and J.P. Ferraris, Chem. Phys. Lett. **277**, 109 (1997).
[18] M.B. Sinclair, D. McBranch, T.W. Hagler, and A.J. Heeger, Synth. Met. **49-50**, 593 (1992).
[19] T. Pauck, R. Hennig, M. Perner, U. Lemmer, U. Siegner, R.F. Mahrt, U. Scherf, K. Müllen, H. Bässler, and E.O. Göbel, Chem. Phys. Lett. **244**, 171 (1995).
[20] R. Jakubiak, C.J. Collison, W.C. Wan, L.J. Rothberg, and B.R. Hsieh, J. Phys. Chem. A **103**, 2394 (1999).
[21] R.G. Kepler, V.S. Valencia, S.J. Jacobs, and J.J. McNamara, Synth. Met. **78**, 227 (1996).
[22] E.S. Maniloff, V.I. Klimov, and D.W. McBranch, Phys. Rev. B **56**, 1876 (1997).
[23] A. Dogariu, D. Vacar, and A.J. Heeger, Phys. Rev. B **58**, 10 218 (1998).
[24] G.J. Denton, N. Tessler, M.A. Stevens, and R.H. Friend, Synth. Met. **102**, 1008 (1999).
[25] T.-Q. Nguyen, I.B. Martini, J. Liu, and B.J. Schwartz, J. Phys. Chem. B **104**, 237 (2000).
[26] A. Köhler, D.A. dos Santos, D. Beljonne, Z. Shuai, J.-L. Brédas, A.B. Holmes, A. Kraus, K. Müllen, and R.H. Friend, Nature (London) **392**, 903 (1998).
[27] D. Moses, A. Dogariu, and A.J. Heeger, Chem. Phys. Lett. **316**, 356 (2000).
[28] C. Silva, A.S. Dhoot, D.M. Russell, M.A. Stevens, A.C. Arias, J.D. MacKenzie, N.C. Greenham, S. Setayesh, K. Müllen, and R.H. Friend, Phys. Rev. B (to be published).
[29] S.V. Frolov, Z. Bao, M. Wohlgenannt, and Z.V. Vardeny, Phys. Rev. Lett. **85**, 2196 (2000).
[30] J. G. Müller, U. Scherf, and U. Lemmer, Synth. Met. (to be published).
[31] G.J. Denton, N. Tessler, M.A. Stevens, and R.H. Friend, Adv. Mater. **9**, 547 (1997).
[32] V. Doan, V. Tran, and B.J. Schwartz, Chem. Phys. Lett. **288**, 576 (1999).
[33] M. Nisoli, S. Stagira, M. Zavelani-Rossi, S. De Silvestri, P. Mataloni, and C. Zenz, Phys. Rev. B **59**, 11 328 (1999).
[34] M.T. Asaki, C.P. Huang, D. Garvey, J. Zhou, H. Kapteyn, and M.M. Murnane, Opt. Lett. **18**, 977 (1993).
[35] R.L. Fork, O.E. Martinez, and J.P. Gordon, Opt. Lett. **9**, 150 (1984).
[36] X. Long, M. Grell, A. Malinowski, D.D.C. Bradley, M. Inbasekaran, and E.P. Woo, Opt. Mater. **9**, 70 (1998).
[37] Y. Shi, J. Liu, and Y. Yang, J. Appl. Phys. **87**, 4254 (2000).
[38] M. A. Stevens, Ph.D. thesis, Cambridge University, 2000.
[39] J.W.P. Hsu, M. Yan, T.M. Jedju, L.J. Rothberg, and B.R. Hsieh, Phys. Rev. B **49**, 712 (1994).
[40] B. Kraabel, D. Moses, and A.J. Heeger, J. Chem. Phys. **103**, 5102 (1995).
[41] J.W. Blatchford, S.W. Jessen, L.B. Lin, J.J. Lih, T.L. Gustafson, A.J. Epstein, D.K. Fu, M.J. Marsella, T.M. Swager, A.G. MacDiarmid, S. Yamaguchi, and H. Hamaguchi, Phys. Rev. Lett. **76**, 1513 (1996).
[42] S.V. Frolov, M. Liess, P.A. Lane, W. Gellermann, Z.V. Vardeny, M. Ozaki, and K. Yoshino, Phys. Rev. Lett. **78**, 4285 (1997).
[43] M. Wohlgenannt, W. Graupner, G. Leising, and Z.V. Vardeny, Phys. Rev. B **60**, 5321 (1999).
[44] A.J. Cadby, P.A. Lane, M. Wolgenannt, C. An, Z.V. Vardeny, and D.D.C. Bradley, Synth. Met. **111**, 515 (2000).
[45] V.I. Klimov, D.W. McBranch, N. Barashkov, and J. Ferraris, Phys. Rev. B **58**, 7654 (1998).
[46] G. Cerullo, S. Stagira, M. Nisoli, S. De Silvestri, G. Lanzani, G. Kranzelbinder, W. Graupner, and G. Leising, Phys. Rev. B **57**, 12 806 (1998).
[47] B.R. Wegewijs, G. Dicker, J. Piris, A. Alba Garcia, M.P. de Haas, and J.M. Warman, Chem. Phys. Lett. **332**, 79 (2000).
[48] A. Haugeneder, M. Neges, C. Kallinger, W. Spirkl, U. Lemmer, J. Feldmann, M.-C. Amann, and U. Scherf, J. Appl. Phys. **85**, 1124 (1999).
[49] S. Stagira, M. Nisoli, G. Cerullo, M. Zavelani–Rossi, S. De Silvestri, G. Lanzani, W. Graupner, and G. Leising, Chem. Phys. Lett. **289**, 205 (1998).
[50] L.M. Herz and R.T. Phillips, Phys. Rev. B **61**, 13 691 (2000).
[51] L.M. Herz and R.T. Phillips (private communication).
[52] N.F. Colaneri, D.D.C. Bradley, R.H. Friend, P.L. Burn, A.B. Holmes, and C.W. Spangler, Phys. Rev. B **42**, 11 670 (1990).
[53] D.S. Ginger and N.C. Greenham, Phys. Rev. B **59**, 10 622 (1999).
[54] S.V. Frolov, P.A. Lane, M. Ozaki, K. Yoshino, and Z.V. Vardeny, Chem. Phys. Lett. **286**, 21 (1998).
[55] M. Yan, L.J. Rothberg, F. Papadimitrakopoulos, M.E. Galvin, and T.M. Miller, Phys. Rev. Lett. **73**, 744 (1994).
[56] A. Haugeneder, M. Neges, C. Kallinger, W. Spirkl, U. Lemmer, J. Feldmann, U. Scherf, E. Harth, A. Gügel, and K. Müllen, Phys. Rev. B **59**, 15 346 (1999).
[57] M. Pope and C.E. Swenberg, *Electronic Processes in Organic Crystals* (Oxford University Press, New York, 1982).
[58] A. Haugeneder, M. Hilmer, C. Kallinger, M. Perner, W. Spirkl, U. Lemmer, J. Feldmann, and U. Scherf, Appl. Phys. B: Lasers Opt. **66**, 389 (1998).
[59] K.S. Wong, D.D.C. Bradley, W. Hayes, J.F. Ryan, R.H. Friend, H. Lindenberger, and S. Roth, J. Phys. C **20**, L187 (1987).

[60] D. Vacar, E.S. Maniloff, D.W. McBranch, and A.J. Heeger, Phys. Rev. B **56**, 4573 (1997).
[61] R.C. Powell and Z.G. Soos, J. Lumin. **11**, 1 (1975).
[62] V. Gulbinas, M. Chachisvilis, L. Valkunas, and V. Sundström, J. Chem. Phys. **100**, 2213 (1996).
[63] T. Förster, Ann. Phys. (Leipzig) **2**, 55 (1948).
[64] T. Förster, Discuss. Faraday Soc. **27**, 7 (1959).
[65] L.N.M. Duysens, Prog. Biophys. Mol. Biol. **14**, 1 (1964).
[66] G. Cerullo, M. Nisoli, S. Stagira, S. De Silvestri, G. Lanzani, W. Graupner, E. List, and G. Leising, Chem. Phys. Lett. **288**, 561 (1998).
[67] A. Dogariu, R. Gupta, A.J. Heeger, and H. Wang, Synth. Met. **100**, 95 (1999).
[68] S.L. Dexheimer, W.A. Vareka, D. Mittleman, A. Zettl, and C.V. Shank, Chem. Phys. Lett. **235**, 552 (1995).
[69] B.I. Greene and R.R. Millard, Phys. Rev. Lett. **55**, 1331 (1985).